Full Length Article

Effects of ageing time on the mechanical and conductivity properties for various round bar diameters of AA 2219 Al alloy

T. Ram Prabhu

CEMILAC, Defence R&D Organization, Bangalore 560093, India

ARTICLE INFO

ABSTRACT

In the present study, AA 2219 alloys of 120 mm round bar are forged into various round bars (25, 50, 75 mm) and subjected to T6 temper heat treatment to identify the peak ageing time for various round bars. The electrical conductivity of the round bars is also measured and correlated with the mechanical properties. It is found that the peak ageing time is 23 h and does not vary up to 75 mm round bar. It increases to 25 h for the 120 mm round bar. The yield and tensile strength of the alloy are found to be in the range of 288–304 MPa and 410–428 MPa for the peak ageing condition. The hardness and conductivity vary in the range of 121–128 BHN and 30–30.96% IACS respectively for the peak ageing condition. Although a near linear relation is found to exist between the strength/hardness and the electrical conductivity values for the selected heat treatment parameters (solution temperature: 535 °C, ageing temperature: 191 °C and the peak ageing time: 23 h), the slope of the curve is different for different round bars. Microstructure characterization studies show the precipitate coarsening with increasing ageing time. Further, precipitate segregation is not found in the microstructure for any cases of round bar diameter and ageing time combinations.

1. Introduction

Al alloys are the most commonly used structural material in the civil and military aircrafts amounting to 60–70% of the primary structure parts. Several properties such as high strength to weight ratio, high specific stiffness, fatigue strength, fracture toughness, and corrosion resistance, matured process technology, easy maintenance in assembly, reasonably good weldability and machinability make this type of alloy as a primary choice for the aircraft designer [1–5]. Among Al alloys, Al–Si, Al–Cu and Al–Zn based alloys are widely used in the aerospace industries. Al–Si based alloys are used in stress non-critical applications such as gear box housing, cylinder blocks, cylinder heads, pistons, engine cooling fans, crank cases, air compressor pistons, fuel pumps, compressor cases, rocker arms and so on [1,3,4,6]. Al–Zn based alloys find applications in stress critical applications such as landing gear, spars, stringers, stabilizer, bulkheads, barrel, struts, axles, fittings, and so on [5,7,8]. Al–Cu based alloys are used in applications such as floor beams, wing box, ribs, covers, brake components, fuel tanks, slot tracks wheel, fittings, fuel systems, body skin connectors, engine pistons and valve bodies [4,8,9]. Among the Al–Cu

alloys, the AA 2219 Al alloy is so special because of its attractive properties such as high specific strength, fracture toughness, weldability and corrosion resistance, reasonable creep strength and superior cryogenic properties. Particularly, the superior weldability and weld strength of this alloy make indispensable in aerospace applications [10]. It is found in the variety of applications such as rocket engine fuel tank, the liquid hydrogen tank, pressure vessel, structural members in the aircraft [1,10]. Most of the applications use this material in sheet and plate forms. Al alloys are usually strengthened by precipitation hardening treatment. The precipitation hardenable alloys should meet two important conditions: (1) the alloying element should have a sufficient solid solubility at high temperature and should exhibit the decreasing solubility with the decreasing temperature characteristics, and (2) the solute should be able to form a fine precipitate that can produce lattice strains in the Al matrix during the ageing treatment. A typical precipitation hardening treatment involves three steps: (1) solution treatment that brings all elements into solid solution state, (2) rapid quenching to avoid diffusion and to retain super saturated solid solution at room temperature, (3) ageing treatment to form fine precipitates by controlled decomposition of metastable super saturated solid solution. The formation of fine precipitates strengthens the alloy through Orowan dislocation strengthening (dislocation cutting through/bypassing over precipitates) mecha-

nism. The coherency, size, interparticle spacing and distribution of the precipitates decide the strength of the alloy. In general, the precipitate should be coherent, fine and uniformly distributed in the matrix to obtain the best strengthening in the alloy. The main process parameters in precipitation hardening treatment are solution treatment temperature and time, quenching medium and severity of quenchant, ageing temperature and time, section thickness. Out of these parameters, temperature and quench effects on section thickness are studied extensively for Al–Cu alloys. Particularly, research studies on the AA 2219 alloy are abundant. Various aspects such as precipitation mechanisms, severe plastic deformation formability, weldability, corrosion, wear, fatigue and creep properties on the AA 2219 alloy have already been explored [11]. The precipitation microstructure and kinetics, ageing sequence was well characterized for various temper conditions (T3, T4, T6, T81, T851, T87 and O) of AA 2219 alloy using differential scanning calorimeter (DSC) and transmission electron microscopy (TEM) for this alloy [12,13].

The area which still needs attention is ageing time effects on mechanical properties of various round bar diameters of the AA 2219 alloy. Excessive ageing time usually leads to overageing by precipitate coarsening resulting in loss of strength. It is noted that the ageing time is not constant with respect to section thickness/diameters in precipitation hardenable alloys. There is a lack of details on ageing time response on the mechanical properties. The measurement of electrical conductivity is an indirect way to understand the nature and distribution of the precipitates in the part as the conductivity is highly sensitive to the chemical composition of the alloy. In general, the addition of any alloying elements into Al reduces the electrical conductivity. Particularly, the alloy which is in solid solution state shows the lowest conductivity. Hence, the alloy when quenched from the solutionizing temperature exhibits the lowest conductivity because the quenching process retains all the alloy elements in solid solution form at room temperature. As the ageing begins, the conductivity initially decreases further low due to the formation of closely spaced GP zones and coherent/semi coherent fine precipitates. As the ageing progresses, the precipitates coarsen due to the diffusion. The conversion of fine semi coherent to coarse incoherent precipitates occurs rapidly leading to the loss of solutes in the matrix. Also, the precipitate coarsening occurs at the expense of neighbor precipitates leading to the wide spacing between the precipitates. These two factors contribute to the rise of conductivity in the precipitate hardenable Al–Cu alloys. As the spacing between particles and/or precipitate size increases, the alloy loses its strength properties due to dislocation bowing (overlooping) mechanisms. The dislocation motion is no longer effectively blocked or resisted by the presence of coarse, widely spaced precipitates leading to the earlier yielding of the alloy. Thus, the precipitate size and distributions in the alloy can be easily analyzed by just measuring electrical conductivity values. Further, the conductivity values help to understand corrosion properties of the alloy. Thus, in the present study, the electrical conductivity measurements are performed to understand the precipitate state in the alloy for various combinations of ageing time and bar diameters.

There have been no detail studies on effects of ageing time response on mechanical properties of the various round bar diameters. Models are currently available to predict non-destructively strength and physical properties using microstructure, hardness and conductivity data. For instance, Guapurich et al. [14] developed a model to relate electrical conductivity and hardness with strength of 7010 Al alloy and found that a non linear relation exists between hardness and strength with electrical conductivity. Starink and Wang [15] used to microstructural data to predict yield strength of a material with a reasonable accuracy. Tiryakioglu et al. [16] and Rosen et al. [17] have used hardness and electrical conductivity data respectively to predict the mechanical properties of AA 2024 and Al–7%Si alloys respectively. Nadan and Chihoski [18] have constructed a graph depicting hardness and conductivity data based on the known quenching and ageing parameters for the AA 2219 alloy. This graph provides a precipitation mechanism for a particular heat treatment condition. This tool is found useful in quality control and failure analysis in bulk production industries as this tool avoids long and time consuming microstructure testing to determine the precipitation state in the alloy. Refaey et al. [19] measured the electrical resistivity of the AA 2024 alloy for the different artificial ageing time correlated with the hardness results. They found that the resistivity increases and attain local saturation due to the GP zones dissolution and later increases till peak ageing time. The resistivity drops above peak ageing time. During the initial phases of precipitation, the ordering events occur by local atom exchanges rather than the bulk diffusion to form GP zones and coherent precipitates. These phases create a multitude of electron scattering centres. These centres increase the resistivity. With the progress of time, the precipitates grow in large sizes that increase the lattice order length larger than the electron mean free path. Thus, the resistivity is decreased above the peak ageing time. Li et al. [20] used electrical conductivity measurements to study the retrogression and reageing heat treatment effects on the stress corrosion cracking and strength properties of 7B04 Al alloy thick plates. Liu et al. [21] studied the addition of Ag in the precipitation hardening behavior of an Al–Cu–Mg alloy having high Cu/Mg ratio using electrical conductivity and hardness measurements combined with TEM and DSC studies for various ageing temperatures. They identified Ω phase as a major precipitate responsible for strengthening in this alloy for the ageing temperature between 170 and 280 °C.

Above studies show that the hardness and electrical conductivity data are sufficient to predict the mechanical properties of Al alloys. In addition, it helps to understand the type, size and distribution of precipitates in the precipitation hardening process. However, experimental works on ageing time response on mechanical properties of different AA 2219 sections are scarce. It is important to understand a relation between the ageing time and the section thickness/diameters to identify the exact time to attain the peak strength properties, as this alloy is one of important structural alloys in the aerospace applications. This alloy is mainly used in plates, sheets, fasteners, extruded sections and forged bar forms in the applications. Besides aerospace applications, this alloy has a significant potential in automobile parts such as body panels, bumpers, engine parts and so on.

In light of this, the present study is undertaken to investigate the effects of ageing time on mechanical properties of various round bar diameters (25, 50, 75 and 120 mm) of the AA 2219 alloy. The main reason for selecting these diameters is that they are representative of typical forging sizes used in the aerospace structural parts such as landing gear barrel, casing, bearing housing, engine mounts, brackets, wing spars, arrester hooks, bulkheads, axles, hubs, struts and brake cylinder. Further, the Al–Cu alloys are quite quench-sensitive. The quench sensitivity problem causes significant properties variations in the thick parts having section/diameters typically $\geqslant$ 120 mm in aerospace applications due to the loss of retained solutes in the solid solution after quenching operation in the precipitation hardening treatment. Thus, the sectional size of the alloy is restricted to usually 120 mm in aircraft structural design. As the heat treatment parameters particularly ageing time is not constant for the sizes even below the 120 mm size, the mechanical properties variation exists among different size ranges if the same heat treatment parameters are used. This indicates that the precipitation kinetics which is responsible for mechanical properties variation vary widely with the heat treatment properties. Hence, it is important to predict the ageing time to obtain

peak strength for the various section diameters. It is prudent to correlate the mechanical properties with the electrical conductivity data to understand the nature and distribution of the precipitates since the conductivity test is non destructive, fast and very simple compared to expensive and time consuming transmission electron microscopy studies. The electrical conductivity data were collected for various round bar diameters and for ageing times. These data are correlated with the hardness and tensile properties.

2. Experimental

An AA 2219 Al alloy extruded bar of 120 mm was selected in the study. The cast billet (diameter: 400 mm and length: 350 mm) was homogenized at a temperature of 480 °C for 24 h before extrusion. The homogenization step eliminates the solute segregations, the low melting phases and coarse precipitates by diffusion, improves the workability and reduces the forging pressure [22]. The billet was extruded in a direct extrusion hydraulic press (30 MN) at a temperature 450 °C. A graphite based lubricant was used to minimize the friction between the container/die and the work piece. The alloy steel flat die preheated to 250 °C was used in the extrusion process. The low extrusion speed of 1 mm/s was selected to avoid excessive heat generation and the surface defects formation. The extrusion ratio selected was 10. The extruded bar was machined to the size of 120 mm × 240 mm to maintain a length to diameter ratio of 2 and also removes the peripheral coarse grain envelope in the extruded surface.

The extruded bars (120 mm diameter) were reduced to three different diameters (25 mm, 50 mm and 75 mm) by open die forging operation in a 5 kN pneumatic power hammer. The forging schematic is shown in Fig. 1(A). The die material selected was H 13 grade hot worked tool steel (Ni–Cr–Mo alloy steel). The bar and the dies were given colloidal form of graphite lubricant coating to minimize the friction and die chilling effects, and to improve the die life. The wet analysis of the alloy gave the following average composition (wt%): Al–6.5%Cu–0.3%Mn–0.25%Zr–0.08%Ti. The bar was heated to 450 °C in an electric resistance type furnace and soaked for 2 h before placing in the die. The die was internally heated by the induction method. The die temperature was maintained at 200 °C to minimize the thermal gradient caused by die chilling. The edges of the bars were blunted to avoid the burr formation. The forging operation was carried out at a temperature of 450 °C. The height reduction ratio/true strain used to obtain 25, 50 and 75 mm in the forging process was 4.8, 2.4 and 1.6/−1.56, −0.87, −0.47 respectively. All the upsetting operations were performed in a single step. The length to diameter ratio of the bars

Fig. 1. (A) Forging method, (B) Sample extraction plan for testing.

Table 1
Soaking time for AA 2219 round bars of various diameters.

Bar diameter (mm)	Soaking time (h)
25	1
50	1.5
75	2
120	3

was sized to 2 by machining after upset forging operations to make the calculation of the soaking time for the solution treatment easy. The forging method and the sample extraction plan for tensile, hardness, microstructure testing was given in Fig. 1(B). The bars were given the following heat treatment cycle.

Step 1: Solution treatment at 535 ± 5 °C and soak it as per Table 1.
Step 2: Quenching in hot water maintained at 60–71 °C and the quench delay time is 3–5 s.
Step 3: Ageing at 191 ± 5 °C for eight different ageing times (20, 22, 23, 25, 26, 27, and 29 h) and air cool to room temperature.

Close temperature control in heat treatment is very essential because too high or low solution temperature causes incipient grain boundary melting or loss of solutes in the matrix respectively. This leads to the loss of strength and ductility properties. The quench delay time should be controlled as minimum as possible to avoid the loss of solute in the matrix or premature precipitation in the critical nose temperature range. The alloy was quenched in hot water to minimize the residual stress in the section which otherwise influences the precipitation kinetics during ageing and also causes warpage or distortion.

The tensile testing was carried out at a strain rate of 10^{-3} s^{-1} in a 25 kN TIRA tensile testing machine. Three samples were tested for tensile properties and the average values were reported. The hardness value was measured in Brinell scale using INDENTEC make universal hardness tester. The indentation time, load and indenter type were 10 s, 612 N and the WC ball respectively. Minimum five readings were measured and the average values were reported. All the testing was performed at room temperature. Samples for microstructure were polished initially by emery papers and followed by velvet cloth polishing with alumina paste to obtain a mirror finish. The polished samples were etched in Keller's reagent (1 ml HF + 1.5 ml HCl + 2.5 ml HNO$_3$ + 95 ml H$_2$O). A Nikon Epiphot optical microscope was used to obtain microstructure images. Testing procedures followed for tensile test, hardness test and microstructure were ASTM E8/E8M, ASTM E10, and ASTM E3/E407 respectively. The electrical conductivity of the heat treated bars was measured and correlated to the stress corrosion cracking susceptibility. The samples were polished to the mirror finish before the conductivity test. The testing was conducted using NOR-TEC 500D (Olympus make) conductivity tester. This instrument was calibrated between 29% IACS and 45% IACS with an accuracy of ±1% IACS according to the ASTM E92-82 standard before the actual test.

3. Results and discussion

3.1. Tensile properties and hardness

The yield and tensile strength results with the ageing time for various round bars of the AA 2219 alloy are presented in Figs. 2 and 3. The rise and drop trend of yield and tensile strength clearly shows that the precipitation reaction occurs completely in all the cases. The rising part of the curve indicates the formation of GP zones and intermediate coherent precipitates (θ'', θ'). The coherent
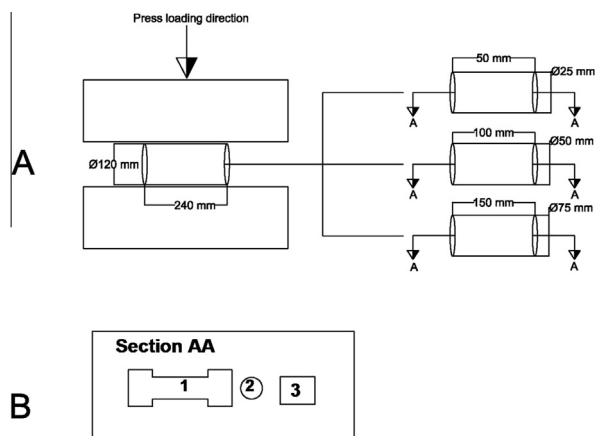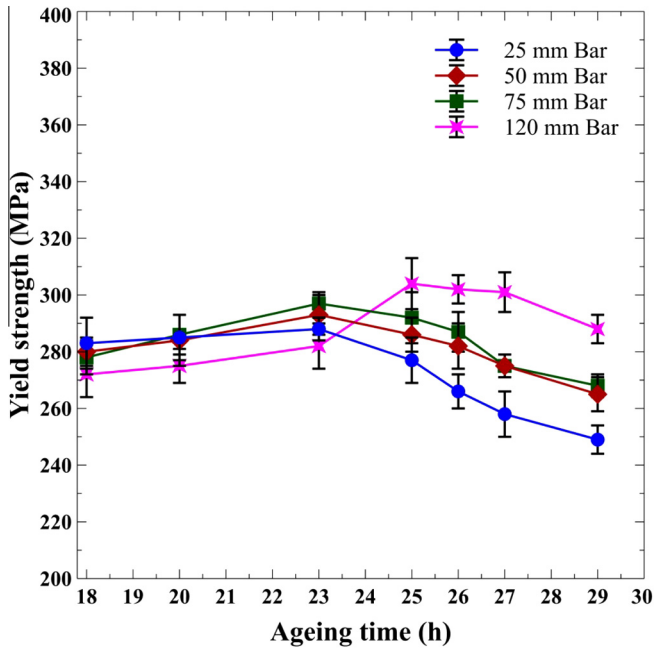
Fig. 2. Variation of yield strength with the ageing time for various round bars (25, 50, 75 and 120 mm) of AA 2219 alloy.
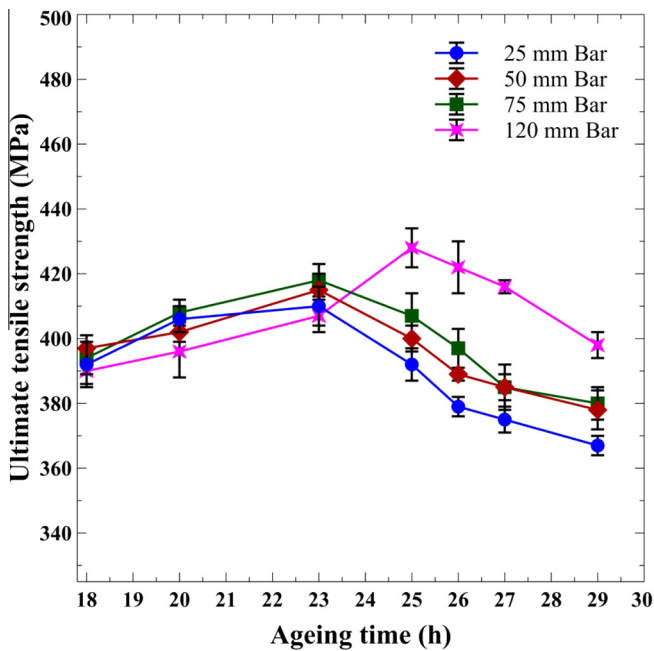
Fig. 3. Variation of ultimate tensile strength with the ageing time for various round bars (25, 50, 75 and 120 mm) of AA 2219 alloy.

strains around the fine precipitates effectively block the motion of gliding dislocations and improve the strength of the alloy in addition to the chemical hardening, lattice friction stress contribution [23]. The coherent strains come from the gradually increasing internal stresses around the GP zones and fine coherent precipitates. The relative amount of $\theta'' + \theta'$ precipitates decides the peak strength in the alloy rather than the coherency associated with lattice strains [18,24,25]. The dropping part of the curve indicates the loss of coherency and coarsening of the precipitates. The time to attain peak strength varies slightly with the bar diameter. For bar diameters 25–75 mm, the peak strength is reached at the ageing

time of 23 h. For the 120 mm extruded bar, the ageing time is about 25 h.

The yield (YS) and tensile strength (UTS) of the alloy are in the range of 288–304 MPa and 410–428 MPa for the peak ageing condition. The slightly higher strength and the right shift of peak ageing time observed in the 120 mm bar are attributed to the process variation. For instance, the comparison of the properties of low and high diameter bars (25 and 120 mm) gives some important results. The process condition of 120 mm bar was extruded against the process condition of 25 mm which is forging. In the case of 25–75 mm bar, the forging direction was normal to the grain flow direction of the extruded input material. This causes the reorientation of the grain flow in the forged structure. The grain flow variation and slightly higher grain growth, as seen in Fig. 9, are responsible for the observed less strength or hardness properties of the 25 mm bar. Comparison of the ratio of YS/UTS for the different phases of ageing, the ratio approaches a maximum at the peak ageing time and then decreases in the overageing phase. This result is in agreement with the results observed for AA 7010 alloy [14].

Similar trends are observed in the hardness results as shown in Fig. 4, although the scatter in the hardness values is higher as seen from the error bar values. The hardness varies in the range of 121–128 BHN for the peak ageing condition. Fig. 5 shows the variation of the ductility with the ageing time for various round bars (25, 50, 75 and 120 mm) of AA 2219 alloy. The ductility decreases with the peak ageing time for all the bars. This is due to the loss of solute from solute enriched matrix to form atomic clusters (GP zones) and fine coherent precipitates (θ'', θ'). At the peak ageing time, the matrix loses most its solutes and forms closely spaced fine precipitates distributed inside the grains without precipitate free zones or continuous grain boundary precipitation. This structure provides maximum strengthening to the alloy by acting as an effective barrier for dislocation motions. As the dislocations are blocked, the resistance to plastic deformation is high leading to lowering the ductility of the alloy. Above peak ageing time, the morphology of non equilibrium precipitates (θ'', θ') grows to attain the stable, equilibrium state (θ). The growth of the precipitation takes place by the dissolution of the non equilibrium very fine pre-
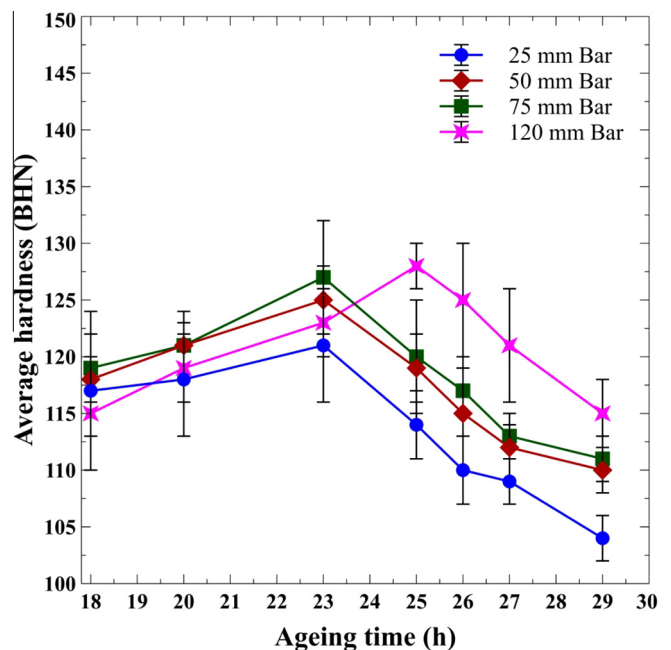
Fig. 4. Variation of hardness with the ageing time for various round bars (25, 50, 75 and 120 mm) of AA 2219 alloy.

5
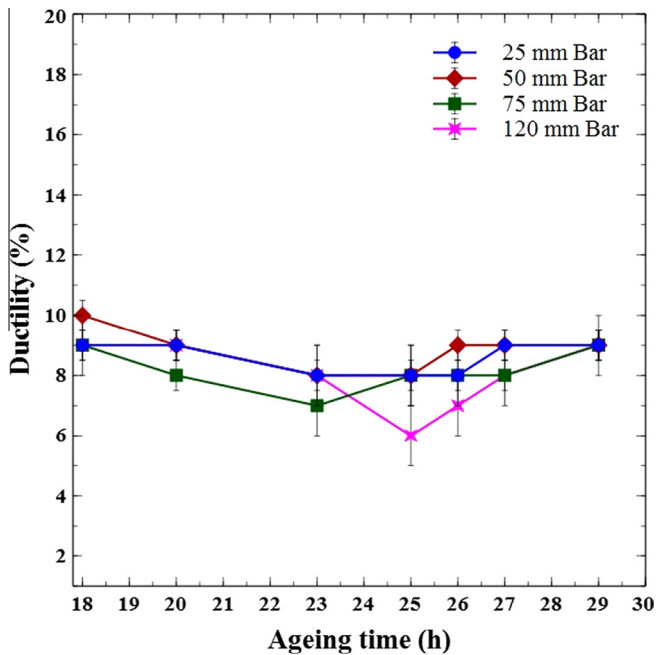
Fig. 5. Relationship between the ductility and the electrical conductivity for various round bars (25, 50, 75 and 120 mm) of AA 2219 alloy.

Fig. 6. Variation of electrical conductivity with the ageing time for various round bars (25, 50, 75 and 120 mm) of AA 2219 alloy.

cipitates and joining with the relatively coarse precipitate. The growth process is driven by the reduction of the interfacial free energy between the particles and the matrix. It is noted that the total volume of the precipitates is constant and only the size of the precipitates increases. This process is called Oswald ripening [23,26,27]. The growth of precipitates results in significant increase of interparticle spacing between particles. Further, the strengthening contribution from the internal lattice strains is also lost due to the precipitate incoherency. The resistance to dislocation motion is significantly reduced due to easy overlooping of dislocation around particles. Further, the matrix is so soft due to the loss of solutes. Thus, strengthening due to solid solution strengthening and precipitation hardening is lost in the alloy. The soft matrix increases the plasticity in the alloy. The ductility begins to increase after peak ageing time in the alloy, as seen in Fig. 5. Comparison among the various diameters of the bar, the time at which the ductility begin to rise varies between 23 and 25 h considering the error bar values. This data corresponds well with the peak ageing time to attain high strength in these bars.

3.2. Conductivity measurements

The results of electrical conductivity for the alloys are presented in Fig. 6. The conductivity is a measure of the phase transformation and the values give an indirect indication of the type, size and amount of precipitate formation. The conductivity of 25–75 mm round bars increases after the ageing time of 23 h except in the time interval between 18 and 20 h for 50 mm round bar. The observed slight increase is attributed to the retrogression effects of some of the formed unstable GP zones. This indicates that the alloy has reached the peak strength at 23 h and begins entering into the overaged stage above 23 h. For the case of 120 mm round bar size, the conductivity decreases up to 25 h and then increases indicating the coarsening of the precipitates. The above results also confirm that the ageing time to reach peak hardening varies slightly above 75 mm. The amount of copper solute in the matrix plays a key in controlling the electrical conductivity of the AA 2219 alloy [18]. After quenching the alloy, the retained super solid solution begins forming precipitates upon ageing. The alloy in the
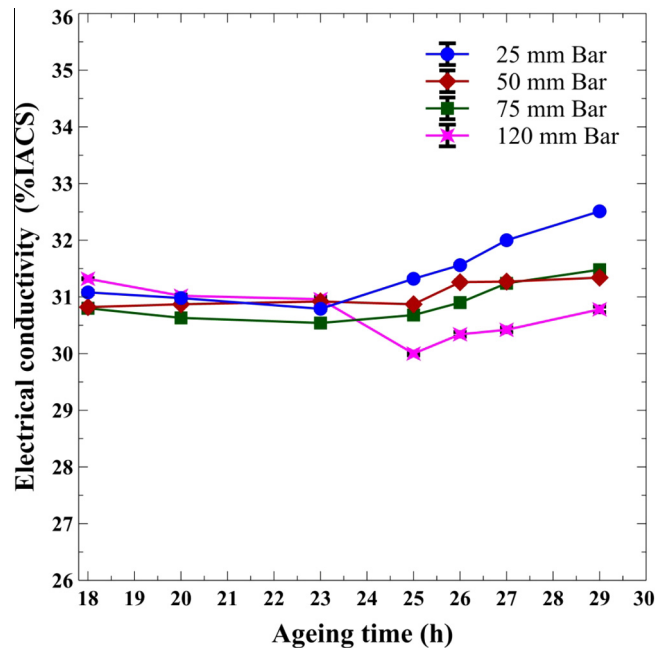
supersaturated solution state has the lowest conductivity due to the decrease of the mean free path of electrons. Two factors which are responsible for the decrease of electron mean free path by affecting the lattice periodicity are: (1) the mismatch of sizes between the solute and the solvent generates several local scattering points, and (2) the electron/atom ratio in the solid solution state is completely different than the alloy in annealed condition [28]. Even with the progress of ageing to remove the solute from the matrix, the conductivity drops due to the scattering of electrons by the formation of coherent G.P. zones and fine non equilibrium precipitates (θ'', θ') up to the peak ageing time. The formation of these precipitates involves the rearrangement of ordered Al and Cu multilayers from the GP zones. The rearrangement causes the disturbance in the lattice uniformity resulting in lowering of the conductivity. Also, the ordering events in these stages to form GP zones and coherent precipitates occur by local atom exchanges rather than the bulk diffusion. These phases create a multitude of electron scattering centres that contribute to the lowering of the conductivity [19]. Between GP zones and the fine semi coherent precipitates, the GP zones are more effective electron scattering phase due to the coherency strain associated with it [14]. Similar results are observed by other investigators [29,30]. Once the precipitates lose the coherency and increase in its size during the overageing phase, the electrical conductivity starts to rise due to significant loss of the solute mainly Cu, from the matrix. Also, the lattice order over length becomes larger than the electron mean free path due to the large precipitate size that helps to increase the conductivity of the alloy [19]. The significant increase of conductivity after the peak ageing time is also observed other researchers in the AA2219 alloy [18,31]. The magnitude of the conductivity loss before peak ageing is relatively insignificant than that of the conductivity gain after peak ageing time, as seen in Fig. 6. This result indicates that conductivity is mainly controlled by the Cu solute present in the matrix rather than the precipitate size or coherency. The conductivity varies in the range of 30–30.96% IACS for the peak ageing condition for all the cases. These results are in agreement with standard % IACS values (30%) reported for AA 2219 T6 alloys in the ASM handbook [27]. Less variability in the conductivity suggests that the size and distribu-

tion of the precipitates are similar for all the round bar sizes in the peak aged condition. The change of slope after the peak ageing time is not constant with increasing ageing time for all cases. The slope is relatively steeper for the case of 25 mm round bar. The higher increase of electrical conductivity corresponds well with strength loss in the 25 mm round bar size case. It indicates that the precipitate coarsening rate is greater for 25 mm round bar size.

The relationship between hardness and tensile strength with the electrical conductivity is given in Figs. 7 and 8. Considering the data up to peak ageing time for various round bars, the near linear sloping downward trend is observed between the hardness/tensile strength and the electrical conductivity in the peak ageing region. It suggests that the gradual conversion of super saturated solid solution to G.P. zones and semi coherent precipitates occurs supporting the precipitation hardening in the alloy. Due to the coherent strains associated with the G.P. zones and coherent fine precipitates, electrons are scattered severely causing the reduction of the electrical conductivity of the alloy [14]. Similar linear trend is not seen between the hardness/tensile strength and the electrical conductivity for the data above/below the peak ageing time. However, the decrease of the slope of the curve above the peaking ageing time is indicative of precipitate coarsening. Similar inverse relation between the hardness and the electrical conductivity was reported in the overageing phase of the AA 7010 alloy [14]. The loss of coherency of precipitates in other words, the loss of internal lattice strains, the significant loss of solute, particularly Cu, from the matrix and the reduction of the number of precipitates make the electron scattering less effective resulting in an increase in the electrical conductivity in the overaged phase. The electrical conductivity of the alloy is also affected by the quantity of copper solute retained in the solid solution. The electrical conductivity reduces with an increase of copper solute in the solid solution. In overageing phase, higher removal of copper solutes from the solid solution to form coarse equilibrium precipitates (θ) also helps to increase the electrical conductivity of the alloy [18]. Further, the slopes of the curve for various round bars are not identical. This suggests that the precipitation mechanism and kinetics are different for different round bars. Comparison of
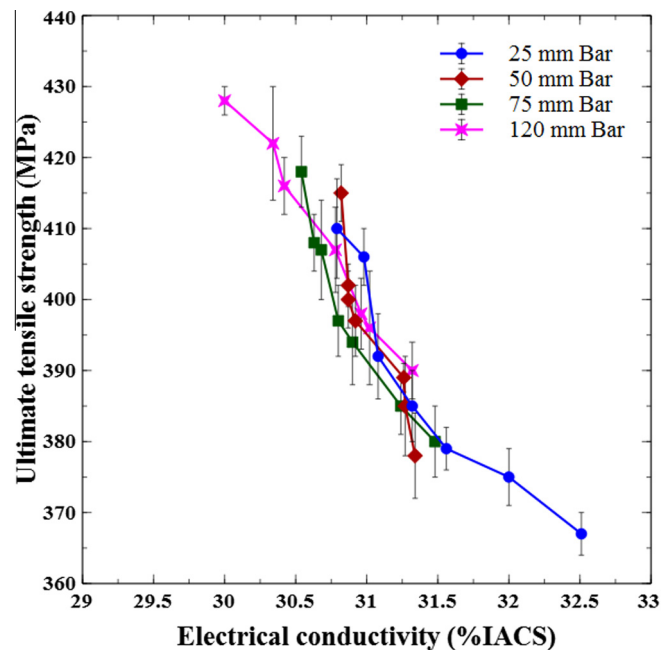
Fig. 8. Relationship between the tensile strength and the electrical conductivity for various round bars (25, 50, 75 and 120 mm) of AA 2219 alloy.

120 mm extruded bar and 25 mm forged round bar results gives few important points: (1) the slope of the strength/hardness with the conductivity for the 25 mm round bar is relatively steeper than that of the 120 mm round bar. Steeper slope observed in the 25 mm round bar indicates that the precipitation kinetics is relatively faster. This comes from the fact of low sectional diameter and higher internal stresses generated from the quenching. Structural refinement and higher dislocation density through higher working by forging also contribute to the precipitation kinetics. It is reported that the increase of dislocation density expedites the kinetics by enhancing Cu diffusivity and the growing ledge density and providing several randomly oriented diffusive paths [13]. The relatively less variation in the hardness/strength data in the underageing stages shows that the rate of the precipitate formation is relatively uniform across the 25 mm round bar section and the uniformity of retained solutes in the solid solution after quenching across the round bar section is also better. Also, the premature formation of precipitates during quenching is also expected to be very less due to smaller sectional diameter, (2) the slopes in the overageing stages are nearly similar for both the cases. The observation of nearly similar slopes in the overageing stages for both the round bars indicates that the precipitation kinetics are nearly similar and the maximum size of the equilibrium precipitates formed in the overageing is nearly same or in other words, the removal rate of retained solute especially Cu from the matrix above the peak ageing time is nearly same, (3) the variation of the hardness data in the underageing stages is higher for the 120 mm round bar. The relatively higher variation of hardness in the underageing stage of 120 mm round bar is probably due to the non uniformity in the sequence of precipitates formation in the thick extruded bar. As the hardness measurement is based on local deformation, it may be possible that the hardness varies depending on the locations of indentation. It is expected that the precipitation kinetics is faster in the surface than the core owing to the thermal conductivity effects. This results in advanced start of precipitation sequence in the surface. This creates the non uniformity in the phases from the surface to the core at any particular ageing time. This non-uniformity is translated into the observed high variation of the hardness in the 120 mm round bar, as seen in Fig. 7. Also, the
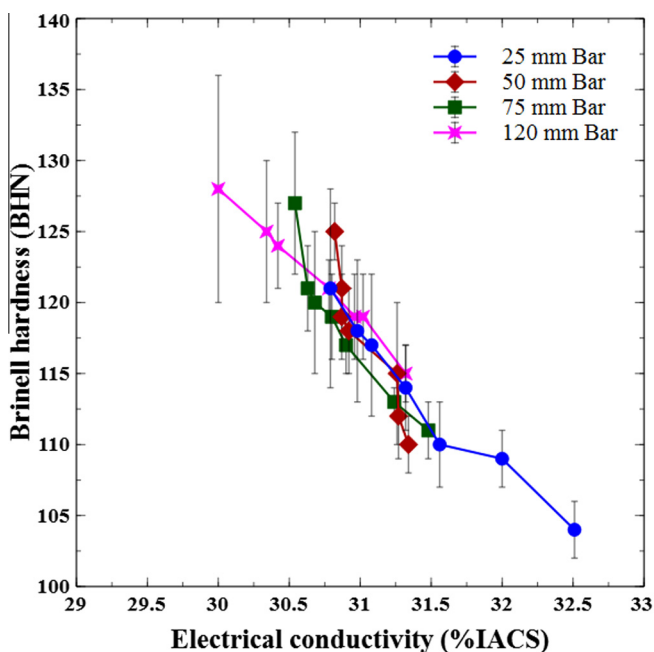
Fig. 7. Relationship between the hardness and the electrical conductivity for various round bars (25, 50, 75 and 120 mm) of AA 2219 alloy.
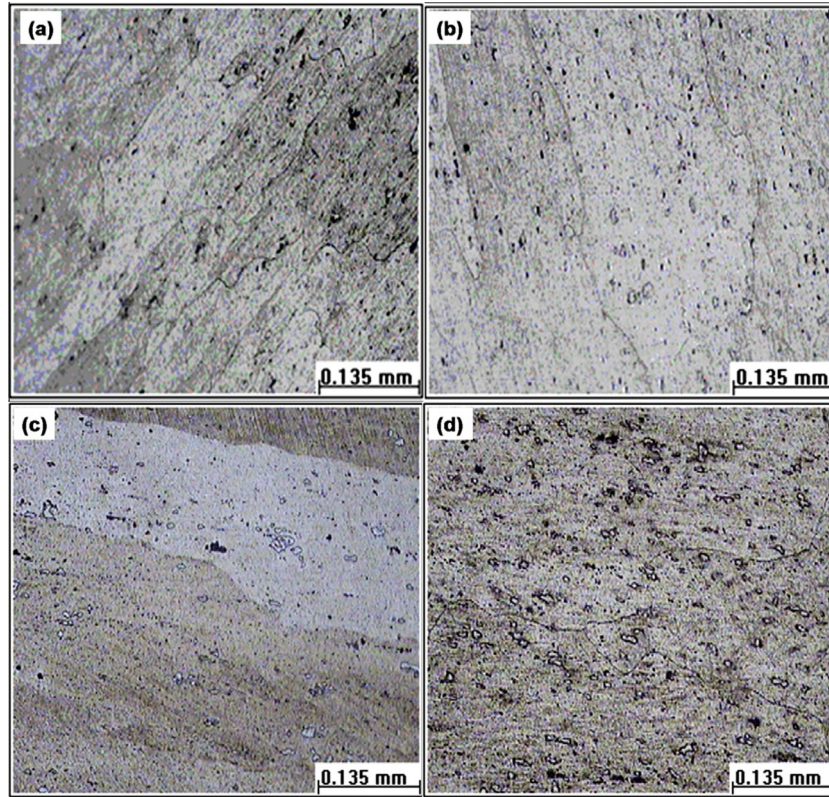
Fig. 9. Microstructure at the ageing time of (a) 20 h, (b) 23 h, (c) 25 h, and (d) 27 h for the round bar diameter of 25 mm.
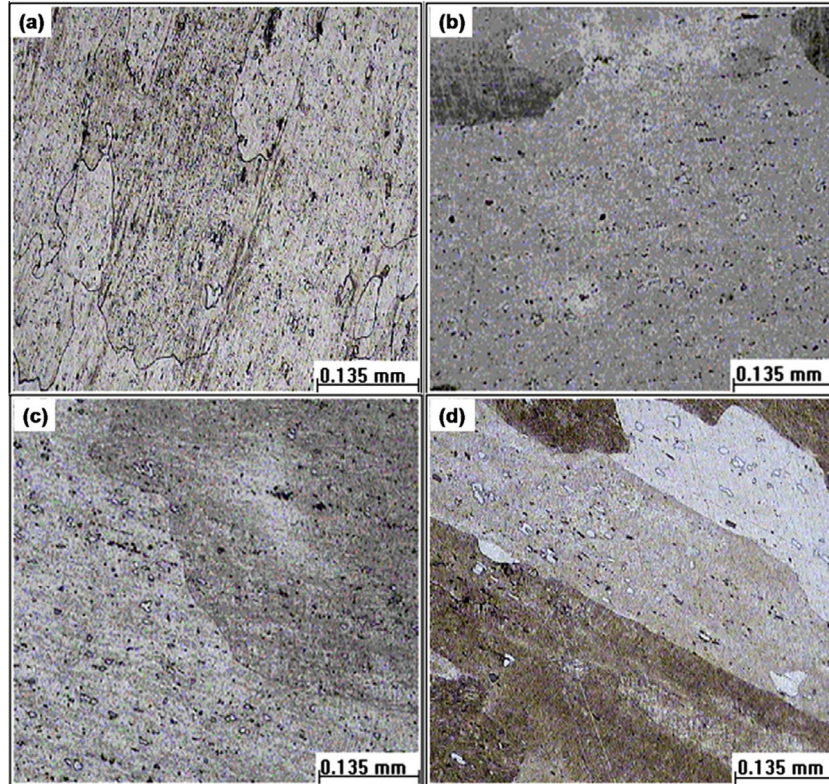
Fig. 10. Microstructure at the ageing time of (a) 20 h, (b) 23 h, (c) 25 h, and (d) 27 h for the round bar diameter of 50 mm.

extruded microstructure contributes to the non uniformity in the precipitation by the largely elongated grain structures. Looking at the tensile strength variation in the underageing stages of the 120 mm round bar, the error bar variation is not so significant, as seen in Fig. 8, indicating that the strength properties are evaluated in global giving the whole properties of the sample. and (4) the rel-
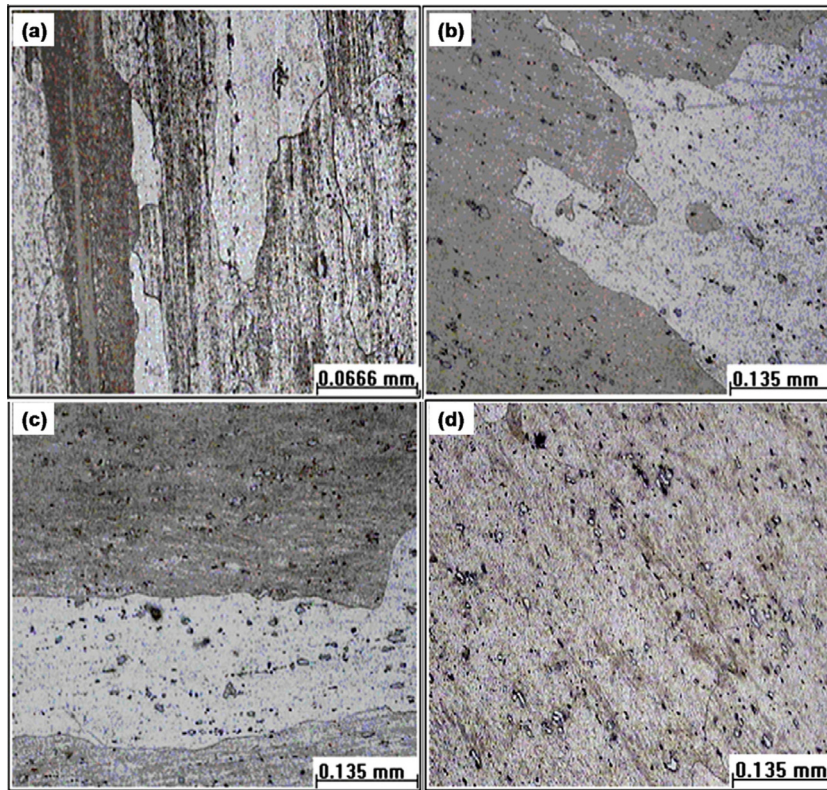
Fig. 11. Microstructure at the ageing time of (a) 20 h, (b) 23 h, (c) 25 h, and (d) 27 h for the round bar diameter of 75 mm.
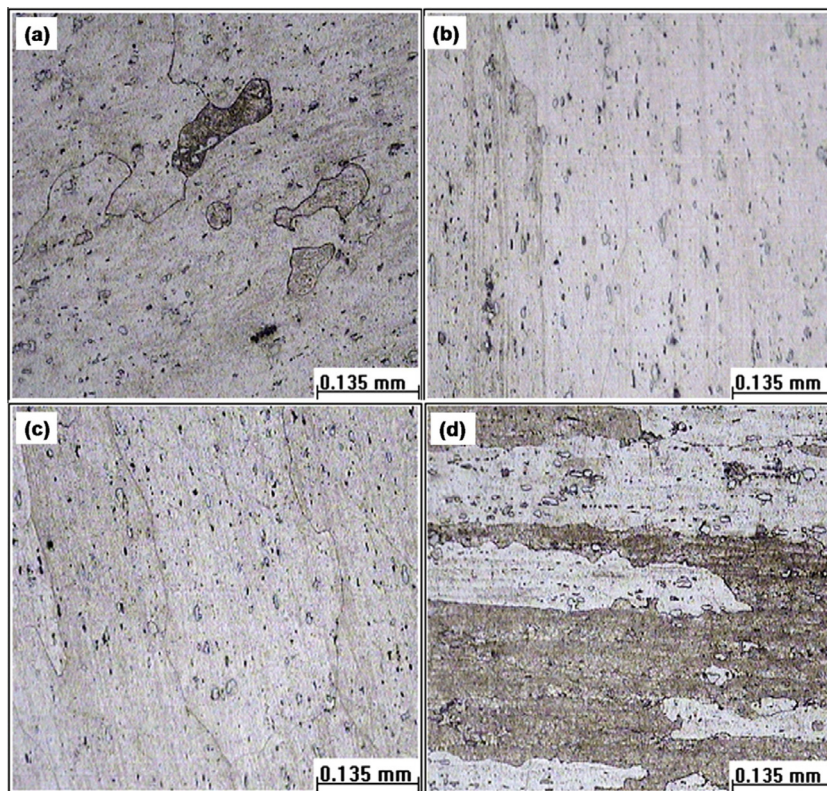
Fig. 12. Microstructure at the ageing time of (a) 20 h, (b) 25 h, (c) 26 h, and (d) 29 h for the round bar diameter of 120 mm.

atively higher value of conductivity for the 25 mm round bar in the overageing indicates that the best possible solute removal from the matrix and the largest possible precipitate size stages are attained whereas, for the 120 mm round bar, further ageing time is required to attain this state, and this result is indicative of faster kinetics of precipitation reaction in the 25 mm round bar. A detail TEM study at various stages of precipitation hardening process is required for both the bars to quantify the amount, nature and state of precipitates formed and to understand the precipitation kinetics. This study is out of scope of the present work. Guapurich et al. [14] and Koch et al. [32] have reported nearly similar non linear trend between the strength and the electrical conductivity in the AA 7010 alloy and AA 7075 alloy respectively.

3.3. Microstructure

The AA 2219 alloy undergoes following precipitation reaction during ageing process [33–35]:

$SSSS \rightarrow$ Cu rich Guinier-Preston zones

$\rightarrow$ Coherent Al_2Cu precipitate (θ'')

$\rightarrow$ Semi-coherent Al_2Cu precipitate (θ')

$\rightarrow$ Equilibrium incoherent Al_2Cu precipitate (θ) (1)
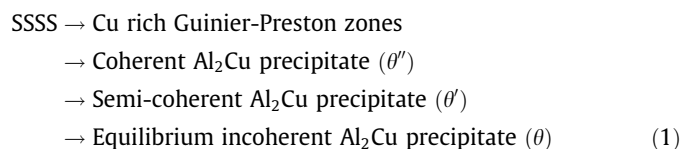
The above reactions show that both coherent GP Zones, and semi coherent θ' are responsible for peak hardening in this alloy. The GP Zones are the first phases to form in the ageing process. It was found from the TEM study that the GP Zones of 10 nm size are formed on the {200} planes in the <100> directions in the α-Al matrix and have a disc shape [18]. A TEM measurement on 50 GP zones in the AA 2219 provides the average size of 3.9 ± 0.4 nm [13]. Nicholson and Nutting [36] reported that the GP zones form as a disc having the diameter of about 5 nm with 1–2 atomic layers thick. Selected area electron diffraction studies on the AA 2219 alloy confirm the coherency and presence of lattice strains on the matrix [18]. The nucleation of the intermediate precipitates occurs preferably on dislocations [35]. With the progress of ageing, the θ'' gradually form on {100} habit planes [18,37]. Papazian [12] observed the θ'' precipitates formation on {110} planes in the AA 2219 alloy by TEM studies. Later, the θ' precipitates begin to form by the θ'' precipitate dissolution with the increase of ageing time. The growth of intermediate precipitates (θ'', θ') takes place by interface lengthening and thickening mechanism controlled by diffusion and the strain field around the coherent faces [13]. These precipitates are identified to have a disc shape and have misfit dislocations on the interfaces [18]. The diameter and thickness of the precipitates are found to be about 20–30 nm and 1.5–2.5 nm respectively [18]. A detail DSC studies on precipitation endo/exothermic reactions and their rates effects of heating rate on GP zones dissolution, reaction rates and precipitation sizes of AA 2219 were reported in [13,18]. Readers are requested to refer the above literatures for detail. Fine size and close spacing of these precipitates provides the significant strengthening by Orowan mechanisms. This time duration is identified as peak ageing time and ideally used to obtain the peak strength in the alloy. The increase of ageing time beyond peak ageing time causes the conversion of semi coherent precipitates (θ') to incoherent equilibrium precipitates (θ) and also the dissolution of G.P. zones. Besides losing the coherency, the equilibrium precipitates are big in size and sparsely distributed. These precipitates are easily by-passed by dislocation. The loss of solute in the matrix makes them very soft. Thus, the material loses strength. As the complete removal of solutes, particularly Cu, from the matrix and sparse distribution of big size precipitates increase the electrical conductivity of the alloy above the peak ageing time.

Figs. 9–12 show the microstructure of the AA 2219 alloy for 25, 50, 75 and 120 mm round bars respectively. In general, the microstructure of the alloys shows a typical elongated grains extruded structure. As seen in Figs. 9–12(a), there are no evidences of resolvable particles below the peak ageing time. Very fine size precipitates are observed in the alloy at peak ageing condition, as seen from Figs. 9–12(b). Once the ageing time reaches beyond the peak ageing time, the microstructure starts revealing the resolvable particles, as seen in Figs. 9–12(c). Particularly, the coarse equilibrium precipitates can be seen after the 4–6 h duration from the peak ageing time, as observed from Figs. 9–12(d). There are no observations of precipitate segregation in the microstructure for any of the stages of ageing condition. The extruded bar microstructure, as seen in Fig. 12, does not show any cast dendritic structure. It shows mainly recrystallized grains. The presence of block like particles in Figs. 9–12(c) and (d) are expected to be Fe or Mn based intermetallic particles. The composition of these particles was found to be Al_7Cu_2Fe and $Al_{20}Cu_2Mn_3$ in AA 2219 alloys by [26,27,38]. These particles have probably formed during the homogenization treatment before the hot extrusion. As the forging and extrusion temperatures are less than the homogenization treatment, these particles are retained in the structure. It is also expected that these particles play a role in inhibiting the recrystallization or grain growth [22]. However, the detail electron microscopy studies help to identify the exact composition of these particles, which is out of the scope of the present work.

4. Conclusions

The size effects on the peak ageing time of AA 2219 alloy were investigated through tensile, hardness and conductivity tests. Key findings from the present study are:

The peak ageing time for the sizes 25–75 mm was found to be 23 h whereas it is 25 h for 120 mm size. The delay in attaining the peak ageing is attributed to the large round bar diameter and the extruded structure which decide the precipitation kinetics.

The yield and tensile strength of the alloy are in the range of 288–304 MPa and 410–428 MPa for the peak ageing condition. The hardness and conductivity vary in the range of 121–128 BHN and 30–30.96% IACS for the peak ageing condition.

Microstructure characterization studies show the precipitate coarsening with increasing ageing time. Further, precipitate segregation is not found in the microstructure for any cases of round bar diameter and ageing time combinations.

A near linear relation existing between the strength/hardness and the electrical conductivity values in the AA 2219 alloy is valid for the selected heat treatment parameters (solution temperature: 535 °C, ageing temperature: 191 °C and the peak ageing time: 23 h). However, the slope of the trend is different for different round bar diameters.

References

[1] F.C. Campbell, Light Weight Materials, 1st ed., ASM International, Materials Park, Ohio, 2012.

[2] I.J. Polmear, Light Alloys: Metallurgy of the Light Metals, 2nd ed., 1989. London.

[3] T. Dursun, C. Soutis, Recent developments in advanced aircraft aluminium alloys, Mater. Des. 56 (2014) 862.

[4] E.A. Starke, J.T. Staley, Application of modern aluminum alloys to aircraft, Prog. Aerosp. Sci. 32 (1996) 131.

[5] T.R. Prabhu, An overview of high-performance aircraft structural Al Alloy-AA7085, Acta Metall. Sin. (Engl. Lett.) 28 (7) (2015) 909–921.

[6] S.G. Irizalp, N. Saklakoglu, Effect of Fe-rich intermetallics on the microstructure and mechanical properties of thixoformed A380 aluminum alloy, Eng. Sci. Technol.: Int. J. (2014) 1–15, http://dx.doi.org/10.1016/ j.jestch.2014.03.006.

[7] T.R. Prabhu, A. Jayathi, A. Kumar, Relationship between the quench delay time and tensile properties for various section thicknesses of extruded AA 7075 Al alloy, Int. J. Microstruct. Mater. Properties (in press).

[8] T.R. Prabhu, Hot forging design and evaluation of the aircraft landing gear barrel Al–Cu alloy structure through simulations and experiments, J. Mater. Eng. Perform. 25 (4) (2016) 1257–1268.

[9] T.R. Prabhu, Mechanical properties, microstructure and fracture surface characterization of thixoforming processed Al–Cu–Mg alloy, Arch. Civ. Mech. Eng. 16 (3) (2016) 335–343.

[10] P.S. Rao, K.G. Sivadasan, P.K. Balasubramanian, Structure–property correlation on AA 2219 aluminium alloy weldments, Bull. Mater. Sci. 19 (3) (1996) 549–557.

[11] S.F. Jia, L.H. Zhan, J. Zhang, Influence of solid solution treatment on microstructure and mechanical properties of 2219 aluminium alloy, Mater. Res. Innovations 18 (2) (2014) 52.

[12] J.M. Papazian, A calorimetric study of precipitation in aluminum alloy 2219, Metall. Trans. A 12A (1981) 269.

[13] J.M. Papazian, Calorimetric studies of precipitation and dissolution kinetics in aluminum alloys 2219 and 7075, Metall. Trans. A 13 (5) (1982) 761–769.

[14] M.A.S. Guapuriche, Y.Y. Zhao, A. Pitman, et al., Correlation of strength with hardness and electrical conductivity for aluminum alloy 7010, Mater. Sci. Forum 519–521 (2006) 853.

[15] M.J. Starink, S.C. Wang, A model for the yield strength of overaged Al–Zn–Mg–Cu alloys, Acta Mater. 51 (2003) 5131.

[16] M. Tiryakioglu, J. Campbell, J.T. Staley, Hardness–strength relationships in cast Al–Si–Mg alloys, Mater. Sci. Forum 331–337 (2000) 295.

[17] M. Rosen, E. Horowits, L. Swartzendruber, et al., The aging process in aluminum alloy 2024 studied by means of eddy currents, Mater. Sci. Eng. 53 (1982) 191.

[18] M. Natan, R.A. Chihoski, Relationship between microstructure, hardness and electrical conductivity of 2219 aluminum, J. Mater. Sci. 18 (1983) 3288.

[19] A.A. Refaey, M.A.A. Rahman, E.A. Badawi, Artificial ageing effect on mechanical, electrical properties and positron lifetime of aircraft 2024 alloy, Defects Diffusion forum 309 (2012) 63–68.

[20] Z. Li, B. Xiong, Y. Zhang, B. Zhu, F. Wang, H. Liu, Improvements in strength and electrical conductivity in 7B04 aluminum alloy pre-stretched thick plates via low-temperature retrogression and re-ageing heat treatments, Mater. Sci. Forum 561–565 (2007) 139–142.

[21] H. Liu, J. Zhang, Q. Liang, H. Hu, Analysis of ageing precipitation behavior of an aluminum alloy, Appl. Mech. Mater. 488–489 (2014) 243–247.

[22] Z. Ahmad, Recent Trends in Processing and Degradation of Aluminium Alloys, InTech Publisher, 2011, http://dx.doi.org/10.5772/741. ISBN 978-953-307-734-5.

[23] G.E. Dieter, Mechanical Metallurgy, McGraw-Hill Publisher, New York, 1961.

[24] F. Fouquet, P. Merle, M. Kohen, et al., Variation du module d'young associee a la precipitation de la phase θ' dans un alliage Al–Cu 4%, Acta Metall. 27 (1979) 315–326.

[25] C. Laird, H.I. Aaronson, Mechanisms of formation of θ and dissolution of θ' precipitates in an Al–4% Cu alloy, Acta Metall. 14 (1966) 121.

[26] J.R. Davis, ASM Specialty Handbook Aluminum and Aluminum Alloys, ASM International, USA, 1993. ISBN: 978-0-87170-496-2.

[27] ASM Handbook, In: Heat treating, 10th ed., vol. 4, ASM International, USA (ISBN-13: 978-0871703798), 1991.

[28] R. Kumar, M. Singh, Electrical conductivity of some aluminium alloys, in: Symposium on Metallurgy of Substitute Ferrous & Non-Ferrous Alloys, 27–30 April, NML, Jamshedpur, 1966.

[29] J.E. Smugeresky, H. Herman, S.R. Pollack, On the nature of the resistivity maximum during Guinier-Preston zone formation, Acta Metall. 17 (1969) 883.

[30] C.W. Bartges, Changes in solid solution composition as a function of artificial ageing time for aluminum alloy 7075, J. Mater. Sci. Lett. 13 (1994) 776–778.

[31] M. Rosen, E. Horowltz, S. Fick, et al., An investigation of the precipitation-hardening process in aluminum alloy 2219 by means of sound wave velocity and ultrasonic attenuation, Mater. Sci. Eng. 53 (1982) 163–177.

[32] G.H. Koch, D.T. Kolijn, The heat treatment of the commercial aluminum alloy 7075, J. Heat Treating 1 (2) (1979) 3.

[33] L.F. Mondolfo, Aluminum Alloys: Structure and Properties, Butterworths & Co. (Publ.) Ltd., London, 1976.

[34] S. Abis, M. Massazza, P. Mengucci, et al., Early ageing mechanisms in a high-copper AlCuMg alloy, Scr. Mater. 45 (2001) 685.

[35] R.B. Nicholson, J. Nutting, Direct observation of the strain field produced by coherent precipitated particles in an age-hardened alloy, Philos. Mag. 3 (1958) 531.

[36] G.W. Lorimer, Precipitation Processes in Solids, 1978. Warrendale, PA.

[37] V.A. Phillips, High resolution electron microscope observations on precipitation in Al–3.0% Cu alloy, Acta Metall. 23 (1975) 751–767.

[38] G.E. Totten, D.S. Mackenzie, Handbook of aluminum, Alloy Production and Materials Manufacturing, vol. 2, Marcel Dekker Publisher, 2003. ISBN-08247-0896-2.